© 2000 Nature America Inc. • http://structbio.nature.com

Structure of the Mad2 spindle assembly checkpoint protein and its interaction with Cdc20

Xuelian Luo[1,3], Guowei Fang[2], Melissa Coldiron[4], Yingxi Lin[1], Hongtao Yu[4], Marc W. Kirschner[2] and Gerhard Wagner[1]

The checkpoint protein Mad2 inhibits the activity of the anaphase promoting complex by sequestering Cdc20 until all chromosomes are aligned at the metaphase plate. We report the solution structure of human Mad2 and its interaction with Cdc20. Mad2 possesses a novel three-layered α/β fold with three α-helices packed between two β-sheets. Using deletion mutants we identified the minimal Mad2-binding region of human Cdc20 as a 40-residue segment immediately N-terminal to the WD40 repeats. Mutagenesis and NMR titration experiments show that a C-terminal flexible region of Mad2 is required for binding to Cdc20. Mad2 and Cdc20 form a tight 1:1 heterodimeric complex in which the C-terminal segment of Mad2 becomes folded. These results provide the first structural insight into mechanisms of the spindle assembly checkpoint.

© 2000 Nature America Inc. • http://structbio.nature.com

The critical task of cell division is to faithfully duplicate the genetic material and then separate it evenly into two daughter cells. To maintain the integrity of the genome, all sister chromatids have to attach to the bipolar mitotic spindle through their kinetochores and align at the metaphase plate. The concomitant separation of the sister chromatids thus allows the inheritance of an identical set of chromosomes in each daughter. A single kinetochore that has not yet been attached to the spindle will delay chromosome segregation and the onset of anaphase[1]. The inhibitory signal on the unattached kinetochores is generated by a surveillance mechanism called the spindle assembly checkpoint or the mitotic checkpoint[2–5].

Several key molecular components of this checkpoint have been identified through a combination of genetic analysis from the budding yeast and biochemical studies from *Xenopus* egg extracts and mammalian cells; these include Mad1–3 and Bub1–3 (refs 6–13). Bub1 is a protein kinase that binds to and phosphorylates Bub3 (refs 12,14). Bub1 and Bub3 seem to act upstream of Mad1 and Mad2 (ref. 15), which also physically interact[9,13]. Mad1 is a large coiled-coil protein (85 kDa) whereas Mad2 is a small protein (25 kDa) of unknown structure; neither contains discernible catalytic domains. Bub2 bears sequence similarity to GTPase-activating proteins (GAPs) of the Rab family small GTPases and is suggested to function in a separate pathway in parallel with Bub1 and Mad2 (refs 16–18). Among these checkpoint proteins, Bub1, Bub3, Mad1 and Mad2 have all been shown to localize to unattached kinetochores in pro-metaphase, suggesting that they are involved in transducing the inhibitory signal originated at these kinetochores[8,9,11,12].

A target of the mitotic checkpoint is the anaphase-promoting complex (APC), which catalyzes the ubiquitination of anaphase inhibitors Pds1, Cut2 or mSecurin, as well as mitotic cyclins to allow the onset of anaphase and subsequent exit from mitosis[5]. The activity of APC is regulated during the cell cycle; it becomes active at the metaphase–anaphase transition and is down-regulated at the G1–S boundary[19]. Activation of APC requires the binding of a WD40 repeat-containing cofactor, Cdc20 (ref. 19). Recently, several lines of evidence have revealed that Mad2 inhibits the APC activity through direct binding to Cdc20 in the APC complex, thus preventing the degradation of anaphase inhibitors until the onset of

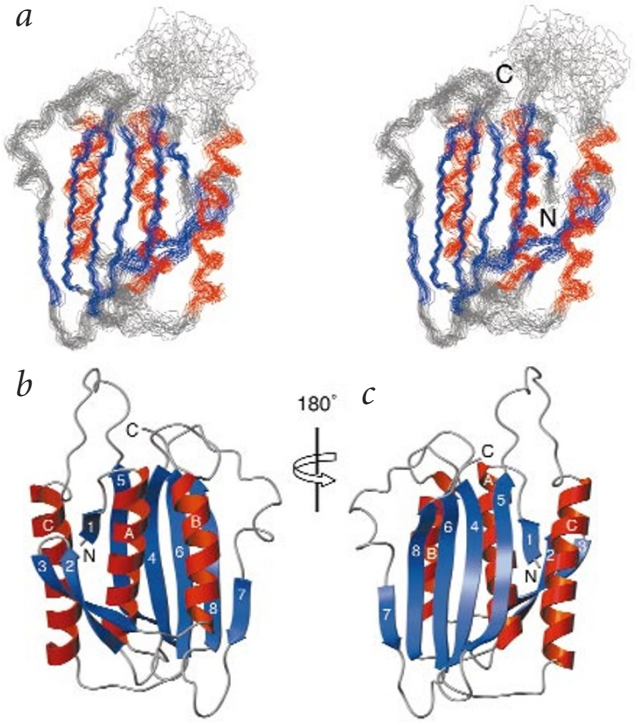

Fig. 1 Mad2 possesses a novel α/β fold. ***a,*** Stereo view of the overlaid backbone traces of the 30 final structures of human Mad2. The β-strands are in blue; α-helices in red; and loops in gray. The N- and C-termini are labeled. The C-terminal residues 196–205 are disordered in solution and are removed for clarity. ***b***, Ribbon drawing of human Mad2. The β-strands are in blue; α-helices are in red; and loops are in gray. N- and C-termini are also labeled. The β-strands are numbers 1–8 and the α-helices are labeled A–C. ***c***, Same as (*b*) but rotated 180° along the y-axis (indicated). Generated with the program MOLMOL[37].

[1]Department of Biological Chemistry and Molecular Pharmacology, [2]Department of Cell Biology, Harvard Medical School, 240 Longwood Avenue, Boston, Massachusetts 02115, USA. [3]Department of Biochemistry, [4]Department of Pharmacology, University of Texas Southwestern Medical Center, 5323 Harry Hines Blvd., Dallas, Texas 75235-9041, USA.

Correspondence and request for materials should be addressed to H.Y. *email: hongtao.yu@email.swmed.edu* or G.W. *email: wagner@hms.harvard.edu*

© 2000 Nature America Inc. • http://structbio.nature.com

anaphase[20–22]. Furthermore, the Mad2 protein expressed in bacteria exists in two conformations, a monomer and an oligomer[22]. Both the monomer and oligomer of Mad2 bind to Cdc20 and inhibit the activity of purified APC^{Cdc20} *in vitro* (Fang and Kirschner, unpublished results). However, only the oligomeric form of Mad2 is active in blocking the APC activity in crude mitotic *Xenopus* egg extracts, suggesting that additional components may modulate the activity of Mad2 *in vivo*[22].

To better understand how Mad2 inhibits the activity of APC, we determined the solution structure of human Mad2 and studied its binding to Cdc20 by nuclear magnetic resonance (NMR) spectroscopy. Mad2 contains a single globular domain and a flexible C-terminal segment. The C-terminal 10 residues of Mad2 are required for its ability both to oligomerize and to bind Cdc20. Binding of Cdc20 disrupts the oligomerization of Mad2 and induces an extensive conformational change in Mad2. Therefore, the formation of a tight 1:1 heterodimer between Mad2 and Cdc20 inhibits the activity of APC^{Cdc20}.

Structure determination

Recombinant wild type human Mad2 protein produced in bacteria was predominantly oligomeric[22]. When the N-terminal 10 amino acid residues were removed, the majority (~75%) of the truncated Mad2 protein (ΔN10-Mad2) existed as monomers[22]. The ΔN10-Mad2 protein inhibited the ubiquitination of cyclin B1 by APC in a reaction reconstituted with purified ubiquitin-activating enzyme (E1), ubiquitin-conjugating enzyme (Ubc-H10), Cdc20 and APC (data not shown). This indicates that the ΔN10-Mad2 retains its biochemical activity. Furthermore, the circular dichroism (CD) spectra of WT-Mad2 and ΔN10-Mad2 are indistinguishable (data not shown). Therefore, ΔN10-Mad2 retains the same tertiary fold as the full-length protein.

Human ΔN10-Mad2 protein was expressed in bacteria as an N-terminal $(His)_6$ fusion protein and purified to apparent homogeneity. With a suite of three-dimensional (3D) triple-resonance experiments acquired on a uniformly $^{15}N/^{13}C/^{2}H$-labeled Mad2 sample, sequence-specific backbone resonance assignment was accomplished by analyzing the observed through-bond connectivities[23]. More than 50% of the side chain resonances were assigned with the HCCH-TOCSY, H(CC)(CO)NH and (H)C(C)(CO)NH spectra performed on a 60% deuterated and uniformly $^{15}N/^{13}C$-labeled protein sample whereas the rest, including the aromatic side chains, were assigned with the help of the ^{15}N-separated or the ^{13}C-separated NOESY spectra. Analysis of these NOESY spectra also identified 2,717 NOEs that were used as distance restraints in the structure calculation. The final 30 structures were calculated by simulated annealing with the program X-PLOR on the basis of 2,897 distance restraints (including 90 hydrogen bond restraints) and 214 dihedral restraints[24]. All structures exhibit good geometry, no violations of distance restraints greater than 0.4 Å, and no dihedral angle violations larger than 5° (Table 1). As evidenced by the higher intensity and narrower line width of their HSQC peaks, the loop connecting β5 and αC (residues 107–121) and the C-terminal 10 residues (Met 196–Asp 205) are flexible in solution. Except for these two regions, the structures are well defined (Table 1).

Mad2 possesses a novel fold

The Mad2 protein forms a single α/β domain with overall dimensions of 45 Å × 35 Å × 25 Å. The structure of Mad2 consists of three layers: a central layer formed by three α-helices, a large six-stranded β-sheet on one side, and a short β-hairpin on the other side (Figs 1, 2*a*). Two hydrophobic cores are created between the three layers of secondary structural elements. An extended hydrophobic core is enclosed by the three α-helices and the main β-sheet. The other side of the β-sheet is completely exposed to solvent. The hydrophobic surfaces of helices αA and αC are effectively shielded from solvent by a highly twisted β-hairpin (β2 and β3), creating the second hydrophobic core. As shown in Fig. 2*a*, the main β-sheet consists of both parallel and antiparallel strands. Helix αA packs against helix αB in an antiparallel orientation whereas helices αA and αC are in a parallel arrangement. Both αA/αB and αA/αC contacting interfaces are extensive, with hydrophobic residues forming interdigitating interactions similar to those observed in helix-loop-helix and leucine-zipper proteins.

A data base search with the DALI[25] server failed to identify significant structural similarities to proteins with known structures, indicating that Mad2 possesses a novel protein fold. A previous report suggested that Mad2 shares sequence and structural similarity with the budding yeast proteins Hop1p and

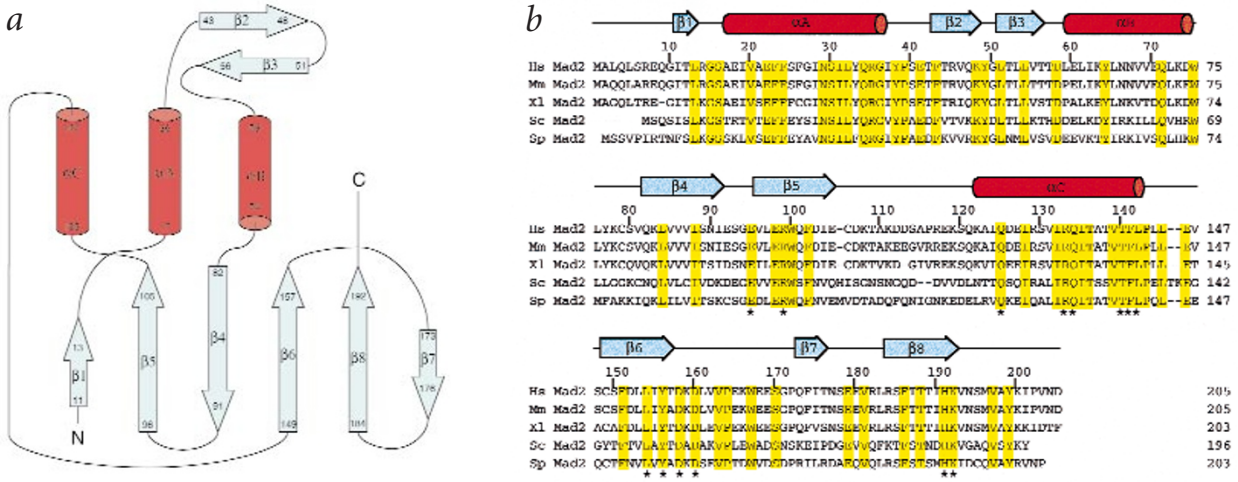

Fig. 2 Secondary structure and sequence alignment of Mad2. ***a***, Topology of Mad2. Strands are shown as arrows and helices are represented by cylinders. The boundaries of the strands and helices are indicated by residue numbers. ***b***, Sequence alignment of Mad2 proteins from various organisms. Hs, *Homo sapiens*; Mm, *Mus musculus*; Xl, *Xenopus laevis*; Sc, *Saccharomyces cerevisiae*; Sp, *Schizosaccharomyces pombe*. The residue numbers of human Mad2 are indicated above the sequence together with the secondary structure elements. The conserved residues are color ed in yellow while the conserved surface residues are labeled by stars. The alignment was performed using the program MegAlign with the CLUSTAL method.

© 2000 Nature America Inc. • http://structbio.nature.com

© 2000 Nature America Inc. • http://structbio.nature.com

Rev7p[26]. In light of our Mad2 structure, it seems that many residues located at the regular secondary structure elements are relatively conserved among these proteins. In particular, Arg 35 and Glu 98 of human Mad2 are invariable among all aligned proteins. They form a salt bridge buried in the interior of the Mad2 structure, suggesting that they are conserved for structural purposes. Taken together, Rev7p, the Mad2-like domain of Hop1p, and the Mad2-like domains of other proteins with unknown functions are likely to possess the same tertiary fold as Mad2.

Residues 111–150 of Cdc20 sufficient for Mad2 binding

Mad2 inhibits the APC activity through direct binding to Cdc20 and forming a ternary complex of Mad2–Cdc20–APC[22]. We next analyzed the interactions between Mad2 and Cdc20 by NMR and mutagenesis. Because the Mad2-binding motif of Slp1, the fission yeast Cdc20 homolog, has been mapped to a 66-amino acid domain adjacent to the WD40 repeats[20], we constructed a series of truncation mutants of human Cdc20 that correspond to a similar region. These mutants were expressed as glutathione-*S*-transferase (GST) fusion proteins in bacteria, purified on glutathione beads, and tested for their ability to interact with human Mad2. As shown in Fig. 3*a*, a Cdc20 fragment consisting of residues 111–150 is sufficient for Mad2-binding. This Cdc20 peptide was then cleaved off GST with thrombin, separated from GST, and used for subsequent NMR titration studies.

Mad2 and Cdc20$_{111–150}$ form a tight 1:1 complex

To analyze the interactions between Mad2 and Cdc20, we titrated the Cdc20 peptide (residues 111–150) into a 0.5 mM ^{15}N-labeled ΔN10-Mad2 sample and monitored the titration with a series of two-dimensional (2D) heteronuclear single quantum coherence (HSQC) spectra. As the Cdc20 peptide was added, a new set of HSQC signals belonging to the Mad2–Cdc20 complex appeared while the peaks corresponding to the free Mad2 protein became weaker. At a molar ratio of 1:1, the free Mad2 peaks disappeared, indicating that the Cdc20 peptide binds to Mad2 with a 1:1 stoichiometry and that its dissociation rate is slow on the NMR time scale (Fig. 3*b*). The Mad2–Cdc20 complex appeared to be a simple heterodimer without further oligomerization because the linewidths of the HSQC signals from the complex are comparable to those of the free Mad2. Comparison of the HSQC spectra before and after peptide addition revealed that the ^{1}H or ^{15}N chemical shift of the majority of the backbone amide groups underwent dramatic changes. Therefore, binding to Cdc20 induces an extensive and global conformational change of the Mad2 protein rather than a localized structural perturbation. In particular, the signals belonging to the C-terminal residues (196–198 and 201) are shifted and become much weaker in the complex (Fig. 3*e*), indicating that this region no longer adopts a flexible conformation and is involved in binding to Cdc20.

C-terminal tail of Mad2 is necessary for Cdc20 binding

We therefore made a mutant Mad2 protein with both the N- and C-terminal 10 residues truncated (ΔNC10-Mad2). Except for the absence of nine sharp peaks belonging to the C-terminal residues, the HSQC spectrum of ΔNC10-Mad2 looked identical to that of ΔN10-Mad2 (Fig. 3*d*). This indicates that the ΔNC10-Mad2 protein retains the native tertiary fold. However, even at a molar ratio of 2:1 (Cdc20 peptide *versus* ΔNC10-Mad2), the HSQC spectrum of ΔNC10-Mad2 was identical to that taken before addition of the Cdc20 peptide (Fig. 3*c*), indicating that ΔNC10-Mad2 did not bind to Cdc20. This demonstrates that the C-terminal tail of Mad2 is required for Cdc20 binding.

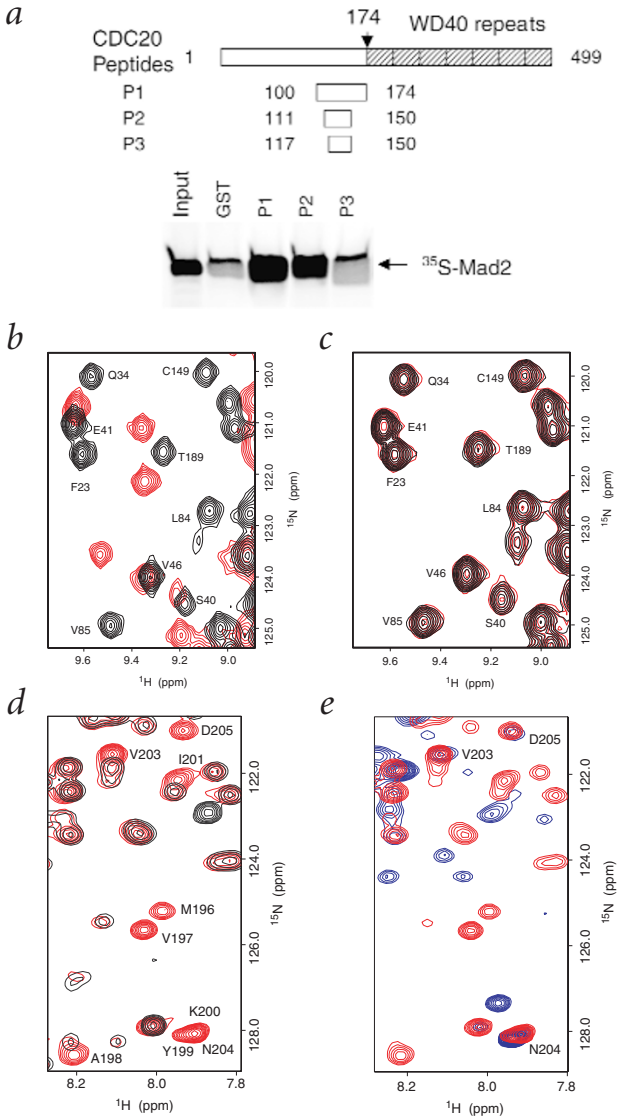

Fig. 3 Interactions between Mad2 and Cdc20. ***a***, The positions of the Cdc20 peptides in the context of the full-length human Cdc20 are shown schematically. Glutathione–Sepharose beads bound with GST-Cdc20 fusion proteins were incubated with *in vitro* translated ^{35}S-Mad2. After washing, the proteins retained on the beads were analyzed by SDS–PAGE followed by autoradiography. The input lane contains 10% of the total Mad2 protein used in each reaction. GST alone was included as a negative control. P2 (111–150) is the smallest fragment that retains Mad2–binding and binds as well as P1 (100–174). The shorter peptide P3 (117–150) does not bind. ***b***, Overlaid sections of HSQC spectra acquired on ΔN10-Mad2 before (in black) and after (in red) addition of the Cdc20 peptide. ***c***, Overlaid sections of HSQC spectra acquired on ΔNC10-Mad2 before (in black contours) and after (in red) addition of the Cdc20 peptide. ***d***, Overlay of the HSQC spectra acquired on ΔNC10-Mad2 (in black) and ΔN10-Mad2 (in red). The peaks belonging to the 10 C-terminal residues are labeled. ***e***, Overlay of the HSQC spectra acquired on ΔN10-Mad2 before (in red) and after (in blue) addition of the Cdc20 peptide. Signals from residues Val 203 (V203), Asn 204 (N204) and Asp 205 (D205) are not perturbed.

Central β-sheet of Mad2 is involved in Cdc20 binding

While the majority of HSQC signals of ΔN10-Mad2 underwent dramatic changes upon Cdc20 binding, there are a few peaks that did not shift significantly. For example, the HSQC signals of Ser 40, Glu 41, and Val 46 only shifted slightly after addition of the Cdc20 peptide (Fig. 3*b*). These residues are located at or near the β-hairpin (strands β2 and β3), which is on the opposite side

© 2000 Nature America Inc. • http://structbio.nature.com

© 2000 Nature America Inc. • http://structbio.nature.com

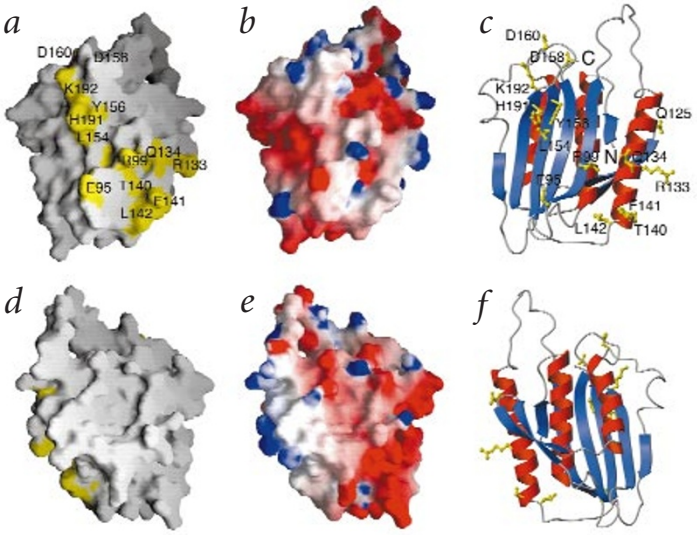

Fig. 4 The Cdc20 binding surface of Mad2. ***a***, Molecular surface of Mad2. The conserved surface residues are in yellow and labeled; the rest are in white. ***b***, Molecular surface of Mad2 in the same orientation as in (*a*) except that it is colored according to electrostatic potential: blue for basic residues; white for hydrophobic residues; and red for acidic residues. ***c***, Ribbon drawing of Mad2 shown in the same orientation as in (*a*) and with the conserved surface residues shown in ball-and-stick models and colored in yellow. ***d–f***, Same as (*a–c*) except that they are rotated 180° along the y-axis. Molecular surfaces were displayed using GRASP[38] and ribbons were generated with MOLMOL[37].

of the molecule to the C-terminal region. This is consistent with the fact that the Cdc20 binding surface is composed of the C-terminal tail and possibly residues at the back of the central β-sheet that are close to the C-terminal region.

Many surface residues of Mad2 are conserved and they form two distinct patches at the back surface of the central β-sheet (Figs 2*b*, 4). One of the patches, formed by residues Leu 154, Tyr 156, Asp 158, Asp 160, His 191 and Lys 192, is in close proximity to the C-terminal tail that is required for Cdc20 binding (Fig. 4*a*,*c*). These residues may also take part in binding to Cdc20. The rest of the conserved surface residues (Arg 133, Gln 134, Thr 140, Phe 141 and Leu 142) are located at or close to helix αC, which is far away from the C-terminal region. This area may be involved in binding to other checkpoint proteins, such as Mad1. Alternatively, it is possible that Mad2 and Cdc20 form multiple interacting surfaces and helix αC represents another contacting site between the two.

Binding of Cdc20 disrupts the oligomerization of Mad2

The oligomerization of Mad2 depends on the C-terminal 10 residues of recombinant Mad2 produced in bacteria, and removal of these residues yielded exclusively monomeric Mad2 protein. Because binding of Cdc20 to Mad2 also requires the C-terminal region, we tested whether Cdc20 binding will disrupt the oligomerization of Mad2 or whether Mad2 oligomers will induce oligomerization of Cdc20. We added the $Cdc20_{111–150}$ peptide to a sample of ^{15}N-labeled wild type Mad2 oligomer. As shown in Fig. 5*a*, the HSQC signals of the oligomeric Mad2 are extremely broad. At a 1:1 ratio of peptide *versus* Mad2 monomer within the oligomer, the HSQC signals become much sharper and well dispersed (Fig. 5*b*). A closer inspection reveals that the HSQC spectrum of the wild type Mad2 in complex with Cdc20 is identical to that of the ΔN10-Mad2–Cdc20 complex, except for several additional peaks belonging to the N-terminal 10 residues. This indicates that the Mad2 oligomer dissociates readily into monomers within minutes of the addition of Cdc20 peptide. Therefore, the Mad2 oligomer does not retain its oligomeric form when complexed to Cdc20. Both the monomeric and oligomeric Mad2 proteins associate with Cdc20 to form heterodimeric complexes with identical conformation.

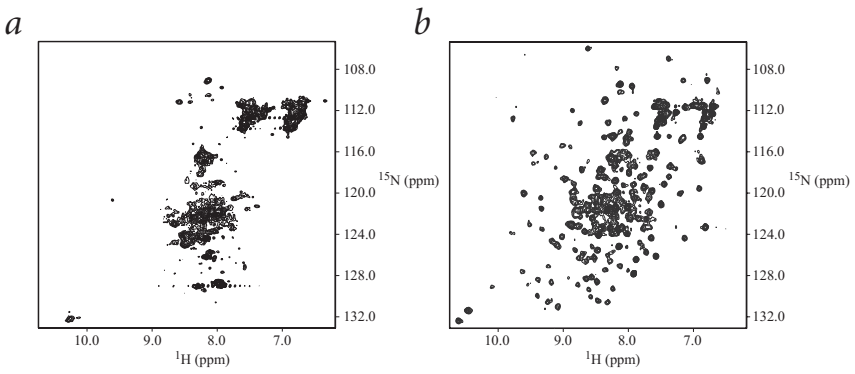

Fig. 5 Cdc20 binding disrupts oligomerization of Mad2. ***a***, the ^{1}H/^{15}N-HSQC spectrum of the Mad2 oligomer. ***b***, the ^{1}H/^{15}N-HSQC spectrum of the same Mad2 oligomer sample taken 10 min after the addition of the $Cdc20_{111–150}$ peptide.

Implications for Mad2 function

The key to deciphering the mechanism of the spindle assembly checkpoint is to understand how a signal from the unattached kinetochore is amplified and distributed throughout the cell to inhibit the activity of APC. Although the nature of this diffusive inhibitory signal is not known, it is clear that for the mitotic checkpoint signal to inhibit the APC activity it has to stabilize the interactions between Mad2 and Cdc20 (ref. 22). When the checkpoint is inactivated, Mad2 is released from Cdc20 to allow APC to degrade anaphase inhibitors[22]. There are two plausible models to explain the checkpoint-dependent association between Mad2 and Cdc20 (Fig. 6). In one scenario, the interaction of Mad2 and Cdc20 requires the presence of other proteins. Depending on the status of the checkpoint, these proteins may stabilize or destabilize the Mad2–Cdc20 association directly by binding or modifying either Mad2 or Cdc20. Alternatively, it is possible that a yet unidentified factor destabilizes the interactions between Mad2 and Cdc20 in the absence of the checkpoint signal. When the checkpoint is activated, a signal generated at the unattached kinetochores acts to inhibit this reversible activity, thus promoting the association of Mad2 and Cdc20. It should be noted that the two models are not mutually exclusive and both mechanisms may exist *in vivo*.

We have previously shown that the Mad2 oligomer, but not the monomer, is active in inhibiting APC in crude *Xenopus* egg extracts, although both forms inhibit the activity of APC efficiently *in vitro*. However, based on our structural studies, the difference in activity between Mad2 monomers and oligomers in crude extracts is not caused, in the case of the oligomers, by the presence of more copies of Mad2 in the Mad2–Cdc20 complex or by induced oligomerization of Cdc20. In fact, both forms of Mad2 bind to Cdc20 as identical 1:1 heterodimeric complexes. We currently do not understand why only the Mad2 oligomer can block the action

© 2000 Nature America Inc. • http://structbio.nature.com

© 2000 Nature America Inc. • http://structbio.nature.com

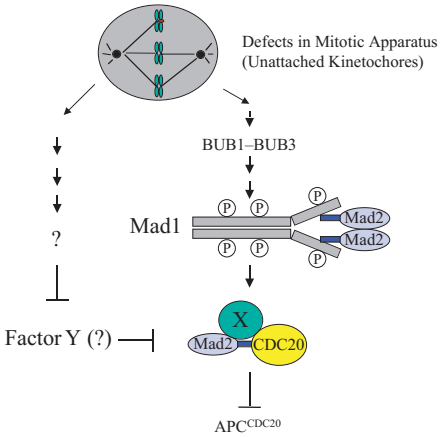

Fig. 6 Hypothetical models for the stabilization of the Mad2–Cdc20 interaction by the spindle assembly checkpoint. An inhibitory signal is generated at the unattached kinetochore (signified by a red dot), which is then transduced by Bub1and Bub3. Bub1 is a kinase that forms a complex with Bub3. Bub1 and Bub3 lie upstream of Mad1 and Mad2, which also interact physically. Mad1 is a coiled-coil protein that can form a homodimer and becomes phosphorylated upon activation of the checkpoint. However, the role of Mad1 phosphorylation is unclear. Mad2 binds to the C-terminal third of the Mad1 protein and this binding requires the C-terminal tail of Mad2. To prevent the activation of the APCCdc20 complex, Mad2 has to associate with Cdc20. In one model, the Mad2–Cdc20 complex is further strengthened by factor X; the binding of factor X to Mad2–Cdc20 is in turn regulated by the checkpoint. In the second model, the binding of Mad2 to Cdc20 is inhibited by factor Y, whose activity is suppressed by the checkpoint. The two mechanisms are not mutually exclusive. Because the C-terminal tail of Mad2 is required for its own oligomerization and for its interactions with Mad1 and CDC20, we speculate that the regulation of Mad2 may involve conformational changes of its C-terminal region.

of APC in crude extracts. It is likely that the functions of Mad2 may be modulated by additional factors in the crude egg extracts, which may preferentially act on either the Mad2 monomers or oligomers. Recently, it has been reported that in yeast, Mad2 binds tightly to Mad1 and this interaction is required for the checkpoint to function[27]. Interestingly, binding between Mad1 and Mad2 also involves the C-terminal tail of Mad2 (ref. 27). Thus, binding of Mad1 to Mad2 may affect the oligomerization status of Mad2 and/or the ability of Mad2 to interact with Cdc20, thereby modulating the activity of Mad2. A complete understanding of Mad2 function will require further biochemical and structural studies that characterize the interactions among Mad1, Mad2 and Cdc20.

Methods

Protein expression and purification. The DNA fragments coding for residues 11–205(ΔN10) and 11–195(ΔNC10) of human Mad2 were subcloned into the *Bam*HI–*Eco*RI site of the pQE-30 vector (Qiagen). Each vector was then transformed into the *Escherichia coli* M15(pREP4) strain (Qiagen) for protein expression. The recombinant Mad2 proteins contain N-terminal 12-residue histidine tags derived from the vector. Uniformly ^{15}N- and/or ^{13}C-labeled Mad2 proteins were prepared by growing cells in M9 minimal media with $^{15}NH_4Cl$ (1 g l^{-1}) and/or [^{13}C] glucose (2 g l^{-1}) as the sole nitrogen and carbon sources, respectively. For triple resonance experiments, uniformly $^{15}N/^{13}C/^{2}H$-labeled Mad2 was produced by growing the cells in M9 media in 99% D_2O. A 60% deuterated and uniformly $^{13}C/^{15}N$-labeled sample was prepared by growing the bacteria in 60% D_2O in M9 media. Selective ^{15}N-labeling was achieved by growing cells in M9 media supplemented with selected ^{15}N-labeled amino acids. The Mad2 proteins were purified by Ni^{2+}-NTA resin according to the manufacturer's protocol followed by anion exchange (Hitrap-Q, Pharmacia) and gel filtration (Sephacryl S-100, Pharmacia) chromatography. The NMR samples typically contained 1.5 mM protein in a buffer of 50 mM sodium phosphate (pH 6.8), 300 mM KCl, 5 mM DTT, 0.04% NaN_3.

NMR spectroscopy. All NMR spectra were recorded on Varian UnityInova 500, Bruker Avance 600 or Varian UnityInova 750 spectrometers at 30 °C. Sequential backbone resonance assignment was achieved using the following three pairs of triple resonance experiments recorded on a uniformly $^{2}H/^{15}N/^{13}C$-labeled sample in H_2O buffer: HNCA / HN(CO)CA, HNCO / HN(CA)CO, and HN(CA)CB / HN(COCA)CB (refs 28–30). In addition, amino acid-selective ^{15}N-labeling was used to confirm the amide proton and nitrogen assignments of lysine, phenylalanine and arginine residues. Side chain resonances were assigned using 3D ^{15}N-TOCSY-HSQC, 3D Cbd-HCCH-TOCSY, H(CC)(CO)NH and (H)C(C)(CO)NH performed with a 60% ^{2}H and uniformly $^{15}N/^{13}C$-labeled sample (refs 31–35). Identification of aromatic side chain spin systems was accomplished using 2D homonuclear TOCSY, DQF-COSY and NOESY experi-

Table 1 Structural statistics for human Mad2[1]

Parameter		SA_i[2]	$<SA>_{ref}$[3]
R.m.s. deviations from experimental restraints			
R.m.s. distance deviations (Å)[4]			
All	(2,897)	0.029 ±0.001	0.032
Interproton distances			
Intraresidue	(821)	0.039 ± 0.001	0.037
Interresidue sequential (|i-j| = 1)	(701)	0.026 ± 0.002	0.044
Interresidue short-range (1<|i-j| ≤ 5)	(492)	0.021 ± 0.002	0.014
Interresidue long -range (|i-j| > 5)	(704)	0.024 ± 0.003	0.019
Hydrogen bond restraints[5]	(180)	0.027 ± 0.003	0.021
R.m.s. dihedral deviations (°)[4]			
All	(214)	0.591 ± 0.093	0.413
Deviations from idealized geometry[6]			
Bonds (Å)	(3,062)	0.003 ± 0.000	0.002
Angles (°)	(5,547)	0.580 ± 0.015	0.522
Impropers (°)	(1,560)	0.448 ± 0.017	0.401
R.m.s. deviations of the 30 structures from the mean coordinates			
Backbone (excluding residues 107–121)		0.90 ± 0.07	
Heavy atoms (excluding residues 107–121)		1.37 ± 0.09	
Backbone (secondary structure)[7]		0.56 ± 0.07	
Heavy atoms (secondary structure)[7]		1.04 ± 0.08	

[1]Excluding the C-terminal residues (196–205).
[2]The SA_i column gives the average and standard deviations for the indicated variables obtained from the 30 final refined simulated annealing structures.
[3]$<SA>_{ref}$ represents the average structure of SA_i least-square fit to each other including all atoms and refined using steepest-descent energy minimization with the simulated annealing parameters.
[4]Distance and angular root mean square (r.m.s.) deviations are from the upper or lower bounds of the distance and angular restraints, respectively, and are calculated relative to the mean structure. None of the calculated structures showed distance violations greater than 0.4 Å or dihedral angle violations greater than 5°.
[5]Each hydrogen bond was interpreted as a couple of distance constraints, d_{NH-O} < 2.3 Å and d_{N-O} < 3.3 Å.
[6]Idealized geometries based on X-PLOR parameters (parallhdg.pro).
[7]Boundaries of secondary structure elements are defined in Fig. 2.

© 2000 Nature America Inc. • http://structbio.nature.com

© 2000 Nature America Inc. • http://structbio.nature.com

ments in D_2O. These systems were then sequentially assigned on the basis of NOEs between the ring protons and backbone amide protons. Stereospecific assignment of methyl groups of valine and leucine residues was obtained from analyzing a 2D ^{1}H-^{13}C-HSQC spectrum performed on a 10% ^{13}C-labeled Mad2 sample[36].

Structure calculation. Interproton distances were derived from a 3D ^{15}N-NOESY-HSQC with a mixing time of 60 ms and a 3D ^{13}C-NOESY-HSQC with a mixing time of 120 ms, both of which were acquired on a Varian 750 MHz spectrometer. NOE connectivities between aromatics and from aromatics to nonaromatic side chains were assigned with the combination of a 2D homonuclear NOESY and a ^{13}C-dispersed NOESY spectra. Crosspeak intensities measured in these NOESY spectra were interpreted as distance constraints based on known distances in regular secondary structural elements. Upper limits for NOE constraints were categorized into four groups; < 2.7 Å for strong, < 3.3 Å (< 3.5 Å for NOEs involving amide protons) for medium, < 5.0 Å for weak, and < 6.0 Å for very weak NOE restraints. An additional 0.5 Å was added to the upper limits for distances involving methyl groups. The lower limits were set to 1.8 Å in all distance constraints. The set of distance restraints was built up in an iterative manner using initial structures generated with only a subset of the total restraints to resolve ambiguities in NOE assignments.

Slowly exchanging amide protons were identified from 2D ^{15}N-^{1}H HSQC spectra recorded 3 h after dissolving the lyophilized protein in D_2O buffer. Each hydrogen bond provided two distance constraints, $d_{NH\text{-}O} < 2.3$ Å and $d_{N\text{-}O} < 3.3$ Å. Backbone ϕ torsional angle restraints were derived from the magnitude of $^{3}J_{NH\text{-}C\alpha H}$ coupling constants that were obtained qualitatively from HMQC-J spectra. The values for ϕ were restricted to ±40° for large $^{3}J_{NH\text{-}C\alpha H}$ coupling constants and ±35° for small $^{3}J_{NH\text{-}C\alpha H}$ coupling constants. Side chain χ_1 angle restraints were assigned based on intraresidue NOE patterns and, in all cases, χ_1 values were restricted to a ±60° range. Three-dimensional structures were calculated from the experimental restraints with the program X-PLOR using standard protocols[24]. The average coordinates of the 30 final structures were minimized using several sets of conjugate gradient energy minimization with gradually increased weight factors for various energy terms[24].

Expression of Cdc20 fragments and Mad2-binding assays. A series of Cdc20 DNA fragments were amplified by PCR and cloned into the pGEX-4T-1 vector (Pharmacia) between the *Bam*HI and *Xho*I sites. Expression of the resulting constructs in BL21 cells produced Cdc20 peptides as GST fusion proteins, which were then purified with glutathione-Sepharose beads (Pharmacia). For Mad2 binding assays, about 200 μg of each GST fusion protein were incubated with 10 μl of glutathione-Sepharose beads to saturate the binding capacity of the beads. The protein-coated beads were then incubated with ^{35}S-Mad2 produced by *in vitro* translation using the Transcription and Translation (TNT) kit (Promega). After washing with phosphate-buffered saline (PBS), the Mad2 protein bound on beads were released by SDS sample buffer, separated by SDS–PAGE and subjected to autoradiography.

Coordinates. The coordinates have been deposited in the Protein Data Bank (accession codes 1DUJ and RCSB01038.

Acknowledgments

We thank J. Rizo for assistance with NMR data acquisition and critical reading of the manuscript. X.L. is the recipient of a postdoctoral fellowship from the National Cancer Institute. G.F. is supported by the Burroughs Wellcome Fund Career Award in the Biomedical Sciences. H.Y. is the Michael Rosenberg Scholar in Biomedical Research and a Damon Runyon Scholar. This work is supported in part by the Damon Runyon Foundation and the Robert A. Welch Foundation (to H.Y.) and the National Institutes of Health (to G.W. and M.W.K.)

Received 14 December, 1999; accepted 21 January, 2000.

1. Nicklas, R.B., Ward, S.C. & Gorbsky, G.J. Kinetochore chemistry is sensitive to tension and may link mitotic forces to a cell cycle checkpoint. *J. Cell. Biol.* **130**, 929–939 (1995).
2. Murray, A.W. The genetics of cell cycle checkpoints. *Curr. Opin. Genet. Dev.* **5**, 5–11 (1995).
3. Hardwick, K.G. The spindle checkpoint. *Trends Genet.* **14**, 1–4 (1998).
4. Nicklas, R.B. How cells get the right chromosomes. *Science* **275**, 632–637 (1997).
5. Nasmyth, K. Separating sister chromatids. *Trends Biochem. Sci.* **24**, 98–104 (1999).
6. Hoyt, M.A., Totis, L. & Roberts, B.T. S. cerevisiae genes required for cell cycle arrest in response to loss of microtubule function. *Cell* **66**, 507–517 (1991).
7. Li, R. & Murray, A.W. Feedback control of mitosis in budding yeast. *Cell* **66**, 519–531 (1991).
8. Chen, R.H., Waters, J.C., Salmon, E.D. & Murray, A.W. Association of spindle assembly checkpoint component XMAD2 with unattached kinetochores. *Science* **274**, 242–246 (1996).
9. Chen, R.H., Shevchenko, A., Mann, M. & Murray, A.W. Spindle checkpoint protein Xmad1 recruits Xmad2 to unattached kinetochores. *J. Cell Biol.* **143**, 283–295 (1998).
10. Li, Y. & Benezra, R. Identification of a human mitotic checkpoint gene: hsMAD2. *Science* **274**, 246–248 (1996).
11. Taylor, S.S. & McKeon, F. Kinetochore localization of murine Bub1 is required for normal mitotic timing and checkpoint response to spindle damage. *Cell* **89**, 727–735 (1997).
12. Taylor, S.S., Ha, E. & McKeon, F. The human homologue of Bub3 is required for kinetochore localization of Bub1 and a Mad3/Bub1-related protein kinase. *J. Cell Biol.* **142**, 1–11 (1998).
13. Jin, D.-Y., Spencer, F. & Jeang, K.-T. Human T cell leukemia virus type 1 oncoprotein Tax targets the human mitotic checkpoint protein MAD1. *Cell* **93**, 81–91 (1998).
14. Farr, K.A. & Hoyt, M.A. Bub1p kinase activates the Saccharomyces cerevisiae spindle assembly checkpoint. *Mol. Cell Biol.* **18**, 2738–2747 (1998).
15. Hardwick, K.G. & Murray, A.W. Mad1p, a phosphoprotein component of the spindle assembly checkpoint in budding yeast. *J. Cell Biol.* **131**, 709–720 (1995).
16. Cuif, M.H. *et al.* Characterization of GAPCenA, a GTPase activating protein for rab6, part of which associates with the centrosome. *EMBO J.* **18**, 1772–1782 (1999).
17. Alexandru, G., Zachariae, W., Schleiffer, A. & Nasmyth, K. Sister chromatid separation and chromosome re-duplication are regulated by different mechanisms in response to spindle damage. *EMBO J.* **18**, 2707–2721 (1999).
18. Li, R. Bifurcation of the mitotic checkpoint pathway in budding yeast. *Proc. Natl. Acad. Sci. U. S. A.* **96**, 4989–4994 (1999).
19. Fang, G., Yu, H. & Kirschner, M.W. Direct binding of CDC20 protein family members activates the anaphase- promoting complex in mitosis and G1. *Mol. Cell* **2**, 163–171 (1998).
20. Kim, S.H., Lin, D.P., Matsumoto, S., Kitazono, A. & Matsumoto, T. Fission yeast Slp1: an effector of the Mad2-dependent spindle checkpoint. *Science* **279**, 1045–1047 (1998).
21. Hwang, L.H. *et al.* Budding yeast Cdc20: a target of the spindle checkpoint. *Science* **279**, 1041–1044 (1998).
22. Fang, G., Yu, H. & Kirschner, M.W. The checkpoint protein MAD2 and the mitotic regulator CDC20 form a ternary complex with the anaphase-promoting complex to control anaphase initiation. *Genes Dev.* **12**, 1871–1883 (1998).
23. Clore, G.M. & Gronenborn, A.M. Determining the structures of large proteins and protein complexes by NMR. *Trends Biotechnol.* **16**, 22–34 (1998).
24. Brünger, A.T. *X-PLOR Version 3.1* (Yale University Press, New Haven, CT, 1993).
25. Holm, L. & Sander, C. Protein structure comparison by alignment of distance matrices. *J. Mol. Biol.* **233**, 123–138 (1993).
26. Aravind, L. & Koonin, E.V. The HORMA domain: a common structural denominator in mitotic checkpoints, chromosome synapsis and DNA repair. *Trends Biochem. Sci.* **23**, 284–286 (1998).
27. Chen, R.H., Brady, D.M., Smith, D., Murray, A.W. & Hardwick, K.G. The spindle checkpoint of budding yeast depends on a tight complex between the mad1 and mad2 proteins. *Mol. Biol. Cell* **10**, 2607–2618 (1999).
28. Yamazaki, T., Lee, W., Arrowsmith, C.H., Muhandiram, D.R. & Kay, L.E. A suite of triple resonance NMR experiments for the backbone assignment of ^{15}N, ^{13}C, ^{2}H labeled proteins with high sensitivity. *J. Am. Chem. Soc.* **116**, 11655–11666 (1994).
29. Matsuo, H., Li, H. & Wagner, G. A sensitive HN(CA)CO experiment for deuterated proteins. *J. Magn. Reson. B* **110**, 112–115 (1996).
30. Matsuo, H., Kupce, E., Li, H. & Wagner, G. Increased sensitivity in HNCA and HN(CO)CA experiments by selective Cβ decoupling. *J. Magn. Reson. B* **113**, 91–96 (1996).
31. Kay, L.E., Xu, G.-Y., Singer, A.U., Muhandiram, D.R. & Forman-Kay, J.D. A gradient-enhanced HCCH-TOCSY experiment for recording side-chain ^{1}H and ^{13}C correlations in H_2O samples of proteins. *J. Magn. Reson.* **B 101**, 333–337 (1993).
32. Matsuo, H., Kupce, E. & Wagner, G. Resolution and sensitivity gain in HCCH-TOCSY experiments by homonuclear Cβ decoupling. *J. Magn. Reson. B* **113**, 190–194 (1996).
33. Grzesiek, S., Anglister, J. & Bax, A. Correlation of backbone amide and aliphatic side-chain resonances in ^{13}C/^{15}N-enriched proteins by isotopic mixing of ^{13}C magnetization. *J. Magn. Reson.* **B101**, 114–119 (1993).
34. Lyons, B.A. & Montelione, G.T. An HCCNH triple-resonance experiment using carbon-13 isotropic mixing for correlating backbone amide and side-chain aliphatic resonances in isotopically enriched proteins. *J. Magn. Reson.* **B 101**, 206–209 (1993).
35. Lin, Y. & Wagner, G. Efficient side chain and backbone assignments in large proteins. *J. Biomol. NMR* **15**, 227–239 (1999).
36. Szyperski, T., Neri, D., Leiting, B., Otting, G. & Wuthrich, K. Support of 1H NMR assignments in proteins by biosynthetically directed fractional ^{13}C-labeling. *J. Biomol. NMR* **2**, 323–334 (1992).
37. Koradi, R., Billeter, M. & Wüthrich, K. MOLMOL: a program for display and analysis of macromolecular structures. *J. Mol. Graph.* **14**, 51–55 (1996).
38 Nicholls, A., Sharp, K.A. & Honig, B. Protein Folding and association: insights from the interfacial and thermodynamic properties of hydrocarbons. *Proteins* **11**, 281–296 (1991).

© 2000 Nature America Inc. • http://structbio.nature.com